Molecular Junctions

Zitierweise: *Angew. Chem. Int. Ed.* **2023,** *62,* e202218640
Internationale Ausgabe: doi.org/10.1002/anie.202218640
Deutsche Ausgabe: doi.org/10.1002/ange.202218640

Chiral Single-Molecule Potentiometers Based on Stapled *ortho*-Oligo(phenylene)ethynylenes

Ana M. Ortuño, Pablo Reiné, Luis Álvarez de Cienfuegos, Irene R. Márquez, Wynand Dednam, Enrico B. Lombardi, Juan J. Palacios, Edmund Leary, Giovanna Longhi, Vladimiro Mujica, Alba Millán, M. Teresa González, Linda A. Zotti,* Delia Miguel,* and Juan M. Cuerva**

Abstract: We report on the chemical design of chiral molecular junctions with stress-dependent conductance, whose helicity is maintained during the stretching of a single molecule junction due to the stapling of both ends of the inner helix. In the reported compounds, different conductive pathways are observed, with clearly different conductance values and plateau-length distributions, attributed to different conformations of the helical structures. The large chiro-optical responses and the potential use of these molecules as unimolecular spin filters have been theoretically proved using state-of-the-art Density Functional Theory (DFT) calculations, including a fully ab-initio estimation of the CISS-originating spin polarization which is done, for the first time, for a realistic molecular system.

Introduction

Molecular electronics is the field of science that studies electron transport phenomena in individual molecules.[1] Within this context, the design and development of molecules capable of reproducing the operation of electronic circuit components, such as wires, transistors, switches, etc. has attracted the attention of scientist of different areas. Beyond the expected benefits of maximal miniaturization, properties derived from quantum effects absent in macroscopic devices can be also explored. To this end, local probes, e.g. the Scanning Tunneling Microscope (STM) and the Atomic Force Microscope (AFM) have been extensively used. Although many of such above mentioned components have been successfully developed in recent years, some of them remain relatively underexplored. Thus, for example, molecular potentiometers, belonging to the mechanoresistive family, are one of them. They incorporate molecules able to change their electrical conductance in response to the application of a mechanical stress.[2] Reported potentiometers are mainly based on linear molecules presenting different conduction channels along the molecular back-

[*] Dr. A. M. Ortuño, Dr. P. Reiné, Prof. L. Álvarez de Cienfuegos, Dr. I. R. Márquez, Dra. A. Millán, Prof. J. M. Cuerva
Departamento de Química Orgánica, Universidad de Granada (UGR), Unidad de Excelencia de Química Aplicada a la Biomedicina y Medioambiente (UEQ), Facultad de Ciencias
C. U. Fuentenueva (Spain)
E-mail: jmcuerva@ugr.es

Dr. W. Dednam, Prof. E. B. Lombardi
Department of Physics, University of South Africa
Science Campus, Private Bag X6, Florida Park 1710 (South Africa)

Prof. J. J. Palacios
Departamento de Física de la Materia Condensada, Instituto Nicolás Cabrera (INC) and IFIMAC, Universidad Autónoma de Madrid
Cantoblanco, 28049 Madrid (Spain)

Dr. E. Leary, Dra. M. T. González
Fundación IMDEA Nanociencia
28049 Madrid (Spain)
E-mail: teresa.gonzalez@imdea.org

Prof. G. Longhi
Dipartimento di Medicina Molecolare e Traslazionale, Universitá di Brescia
Viale Europa 11, 25121 Brescia (Italy)

Prof. V. Mujica
School of Molecular Sciences, Arizona State University
Tempe, AZ 85287 (USA)
and
Kimika Fakultatea, Euskal Herriko Unibertsitatea (UPV/EHU)
P.K. 1072, 20018 Donostia, Euskadi (Spain)

L. A. Zotti
Departamento de Física Teórica de la Materia Condensada and IFIMAC, Universidad Autónoma de Madrid
Cantoblanco, 28049 Madrid (Spain)
E-mail: linda.zotti@uam.es

Prof. V. Mujica, Dra. D. Miguel
Departamento de Fisicoquímica, Universidad de Granada (UGR), (UEQ), Facultad de Ciencias
C. U. Fuentenueva (Spain)
E-mail: dmalvarez@ugr.es

bone, whose transport properties are sensitive to stress thus leading to additional conduction pathways of higher conductance (G) than the corresponding end-to-end pathway. This kind of multichannel compounds can be considered as molecular potentiometers, since the total resistance (typically associated to end-to-end pathways) can be fractionated in contributions connected to shorter pathways. Besides the works of Venkataraman and others using polyenic chains,[3] silicon-containing molecular wires,[4] and thiophenes,[5] we have been pioneers in the development of nitrogen containing para-oligo(phenylene)ethynylene (*p*-OPE) derivatives presenting two and three well-defined conductance states due to a non-symmetrically placed nitrogen in-backbone anchor group.[6]

A less explored strategy is the conformational distortion of a 3D flexible arrangement during the compression-stretching of the molecular junction.[7] In this sense, helical foldamers are privileged scaffolds since they can have significantly different conformers (folded and unfolded) that can present different conductive values. In 2021, Tang et al., proved this idea. In that seminal work, foldamers based on *ortho*-phenylenes were capable of presenting two different conformations showing different conductive eigenchannels (Figure 1, left).[8] Based on that concept, we hypothesized that a covalent stapling of the foldamers would result in a more robust helical structure avoiding any interference of ill-defined fully unfolded structures and, probably, it would improve the identification of the different conductive channels. By avoiding the unfolding process, the absolute configuration of the helix is maintained during the measurements. Each single event would be globally chiral offering the possibility to study the influence of the chirality in a controlled way.

Chirality is an under-explored topic in organic electronics[1] despite the fact that interesting phenomena at the molecular level are expected. Within this context, the CISS (Chirality Induced Spin Selectivity) effect has garnered significant attention in the last few decades. Due to the CISS effect, electron transport through chiral molecular nanowires favors one of the two spin components over the other, thus promoting spin polarization without external magnetic fields and at room temperature. The consensus is that this effect could be exploited for spintronic applications, and the development of molecular-based logic and memory units.[9–11] Nevertheless, few successful examples have been described at single molecule level,[12–14] relaying most of the studies in silico and considering idealized and perfect helical molecules such as carbon chains, polyacetylenes, peptides or helicenes.[15–18] The application of such idealized systems in real measurements is hard to imagine due to the virtually impossible synthetic challenges they present. In this sense, just one example of single-molecule conductivity of an enantiopure oxa[19]helicene derivative has been described.[19] Nevertheless, none of the precedent studies points out the possibility to control the spin polarization by changing the geometry of the unimolecular potentiometer whilst maintaining the absolute configuration of the helical system. The use of peptides, which are intrinsically chiral and have been proposed for CISS studies[20] could be a potential solution. However, they are not very suitable if multiple and well-distinct conductance groups are desired, as peptides are also rich in chemical groups which can bind to the electrodes, gold in this case, at different chemical sites all over their structure.[21] As a consequence, the precise control of different conductance groups during the stretching process would be very difficult as binding could occur through a high number of anchoring points along the molecular bridge.

Non-racemizable enantiopure organic molecule able to modify its three-dimensional structure as a result of an applied electro-mechanical stimulus seems to be the best candidate for these kind of studies. That is, a single chiral molecule could, in principle, adopt different chiral conformations which may also be controlled by a mechanical process.[2,20b–c] In this sense, we recently described new fully conjugated and enantiopure helical architectures based on *ortho*-oligophenylenethynylenes (*o*-OPEs) including a novel control of their chirality.[22] These systems seem perfect scaffolds for our purpose, as they would maintain a remarkable conformational flexibility while remaining chiral even under severe pulling and pushing events owing to the presence of a stabilizing staple. This structural motif would prevent loss of chirality via complete unfolding during the electrical measurements, thus allowing a better identification of different conduction channels. Additionally, the development of these stapled foldamers enables the evaluation of only one enantiomer in the junction. The purpose of this study, therefore, is to explore the possibility of synthesizing stapled *o*-OPEs which, at the same time, i) can form stable junctions in break-junction experiments as well as provide multiple conductance groups, and ii) are chiral and thus suitable candidates for the CISS effect (Figure 1, right). This effort would pave the way to study the influence of chirality on the CISS effect in real helical systems and the development of spin-dependent potentiometers. Theoretical calculations developed in this work validate the potential efficiency of these compounds as candidates for the

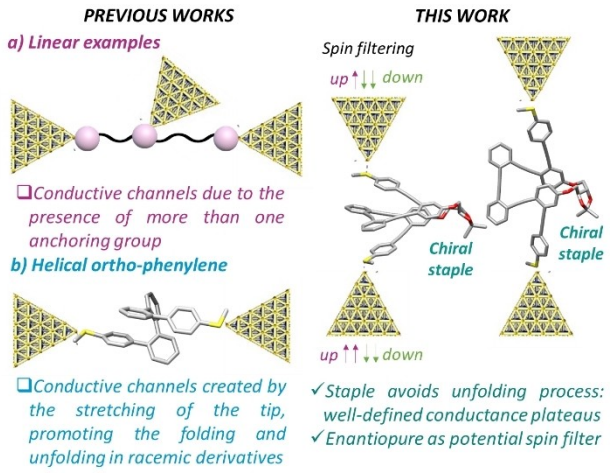

Figure 1. Working hypothesis. Double aim of stapled helical derivatives: avoid complete unfolding processes and allow spin filtering through enantiopure compounds.

occurrence of this phenomenon, including a fully ab-initio estimation of the CISS-originating spin polarization carried out, for the first time, for a realistic molecular system.

This manuscript is organized as follows. First, we report on the chemical synthesis of the compounds, we then explore conductance measurements made using the STM-break-junction technique to determine whether these compounds can form stable junctions and provide different easily distinguishable conductance pathways. Finally, the theoretical evaluation of the electrical conductance and the three-dimensional spin polarization is reported.

Results and Discussion

We designed two prototypical molecules, model compound **1** and enantiopure derivative (*S*,*S*,*P*)-**2** (Scheme 1). The first of these is conformationally unrestricted, analogous to one previously described,[8] but including alkynes between phenyl moieties, thus allowing several interconvertible folded-unfolded conformations that can be adopted during the measurements using the scanning tunneling microscope break-junction (STM-BJ) technique. On the other hand, compound (*S*,*S*,*P*)-**2** represents the most basic structure we can make to test the success of our approach, being the smallest stapled compound with at least one full turn in the helix. This compound has the same number of phenyl rings as **1** but includes a chiral staple to maintain the absolute configuration of the helix during the conductance measurements. That is, the absolute configuration of the inner loop of the molecule is preserved along the experiments. We anticipate that this strategy will help the structure to form well-defined plateaus and prevent its complete unfolding as can happen with **1**. It is worth noting that the chiral staple can efficiently drive the equilibrium to mainly one of the absolute configuration of the helix by a chirality transfer process from the staple to the helical core, i.e. the use of just one enantiomer of the chiral moiety (staple) induces just one absolute configuration.[22] In this case, only the *P* enantiomer is present. It must also be considered that both structures **1** and (*S*,*S*,*P*)-**2** are able to interact with carbophilic metals by means of the five alkynes, thus stabilizing helical structures although not in a permanent way.[22,23]

Both compounds were prepared from simple *o*-OPE skeletons synthesized by a sequence of Sonogashira couplings and trimethylsilyl (TMS) deprotection steps, affording precursors **I** and **II** (Scheme 1). For stapled compound (*S*,*S*,*P*)-**2**, a macrocyclization reaction with enantiopure 1,4-di-*O*-tosyl-2,3-*O*-isopropylidene-*L*-threitol was carried out.[22a] Finally, the incorporation of the required linking groups (thiometyl, -SMe) for STM measurements were made using a coupling reaction with 4-ethynylphenyl methyl thiol (see Supporting Information, section 1). In order to avoid the presence of unwanted minor impurities in the STM experiments, we performed an exhaustive purification by HPLC (traces are shown in Supporting Information, Figures S8–S9), which gave a final purity of almost 99 %.

We have previously described that the (*S*,*S*) configuration of both hydroxyl groups in the staple induces a *P*-biased folding in the helical core,[22,23] which corresponds to a positive Cotton effect of the less energetic band of the circular dichroism (CD) spectra and also according with a single crystal X-ray structure recently described by us.[22b] Considering also the intriguing relationship between the intensity of CD signal and the magnitude of the CISS effect previously reported[24] we decided to evaluate the chiroptical properties of (*S*,*S*,*P*)-**2** both in ground (CD) and excited (circularly polarized luminescence, CPL) states (Figure 2). The experiments showed a rather large CD (and CPL) signal for (*S*,*S*,*P*)-**2** ($\Delta\varepsilon = 12.4\ mol^{-1}\,L\,cm^{-1}$, $g_{abs} = 0.9\times10^{-2}$ at $\lambda = 405$ nm, $g_{lum} = 1.4\times10^{-2}$ at $\lambda = 418$ nm), being these values about one order of magnitude higher than that typical of organic molecules. This fact is in agreement with our previous results, evidencing the stabilization of a folded structure with a prevalent handedness (see Supporting Information, Figure S7 for data in all the spectral range and Table S1 for the values in different solvents).

Being dynamic structures, each compound exists in different conformations in solution whose populations at a given temperature are controlled by the corresponding relative energies. The study of such equilibrium is useful for

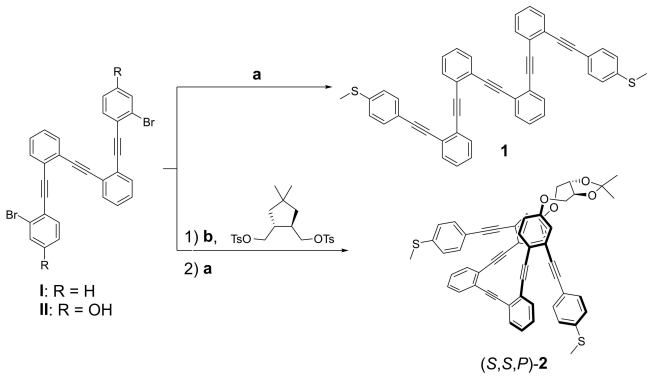

Scheme 1. Synthesis of helical systems **1**-(*S*,*S*,*P*)-**2**. Reagents and conditions: (a) 4-ethynylphenyl methyl thiol, $Pd(CH_3CN)_2Cl_2$, CuI, $PtBu_3\cdot HBF_4$, iPr_2NH/THF, 60 °C, (b) Cs_2CO_3, CH_3CN, reflux. Yields of steps a and b for each derivative are described in the Supporting Information.

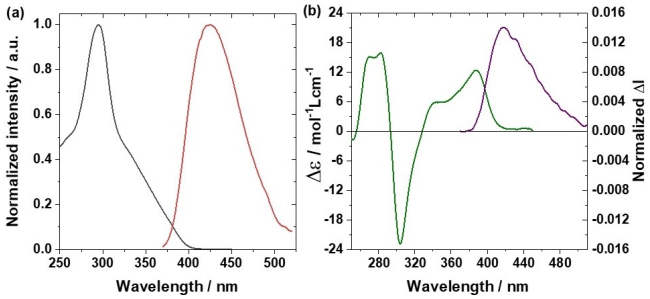

Figure 2. (a) Absorbance (black) and fluorescence (red) and (b) CD (green) and CPL (violet, $\lambda_{exc} = 300$ nm) spectra of compound (*S*,*S*,*P*)-**2** in CH_3CN. For other solvents see Supporting Information (Figures S5–S7 and Table S1).

the understanding of the subsequent STM measurements. Therefore, we carried out a conformational study of compounds **1** and (*S*,*S*,*P*)-**2** with the aid of the CREST tool which is based on a semi-empirical tight-binding quantum chemistry method described by Grimme,[25] DFT optimization was conducted with Gaussian 16[26] at the PBE/cc-pVDZ level with empirical dispersion corrections which are important to account for stacking interactions.[27] Energetics and structure description of DFT calculated conformers are reported in Tables S3 and S4 for **1** and (*S*,*S*,*P*)-**2**, respectively. Conformational analysis of model compound **1** showed a major conformer (82 % population) consisting of a "Figure-of-eight" shaped, partially folded, structure of *MM* or *PP* helicity in the two loops, followed by a fully folded conformation with a considerably lower contribution of 12.5 % and a "half-folded" isomer with less than 5 %. The energy difference between the two most populated structures is just 1.1 kcal mol^{-1}. It needs to be taken into account that in this case each conformation is equally likely in one enantiomer or the other, thus negating its use as spin filter. On the other hand, for compound **2**, the (*S*,*S*) configuration of the acetal group leads to a significant population of the *P* conformers as previously described[23b] and confirmed by CD measurements, with the contribution of *M* stereoisomers being negligible. The presence of such conformational bias is essential for retaining the absolute configuration of the helix, because, otherwise, a racemization process can take place, thus canceling the possibility of using this molecule for spin filtering processes when averaging all the measurements. The presence of the staple greatly simplifies the conformational space in comparison to compound **1** since the "figure-of-eight" shaped and the transplanar (called "completely unfolded" in Table S3) structures are not possible. Among the lowest energy *P* conformers of compound **2** we may classify spatial arrangements as: fully-folded, half-folded and elongated (Figure 3). Although both, theoretical and experimental CD and CPL data suggest the prevalence of a folded geometry with the *P*-handedness, some competition between π–π intramolecular attractive interactions and solute-solvent interactions (difficult to address theoretically) may also be important for real samples: different combinations of previously mentioned conformations may be hypothesized in different solvents. In fact, the high sensitivity of the CD spectra of the chiral molecule in different solvents has been previously observed.[22b] In this case, in the range 300–350 nm different intensities have been obtained when changing the solvent, while the less energetic band shows only some wavelength shift (see Figure S6 in the Supporting Information). The energy difference between the fully-folded and half-folded structures is just 1.2 kcal mol^{-1}, while it is about 10 kcal mol^{-1} between the folded and the elongated structures, which makes this last conformation very scarce (Figure 3).

In order to test the real-world suitability of **1** and (*S*,*S*,*P*)-**2**, we performed transport measurements using a home-made BJ-STM, using gold electrodes. This allows us to cross-check our results with previous reference studies. Firstly we wanted to establish if **1** and (*S*,*S*,*P*)-**2** bind well-enough to give reproducible signatures. Secondly, we wish

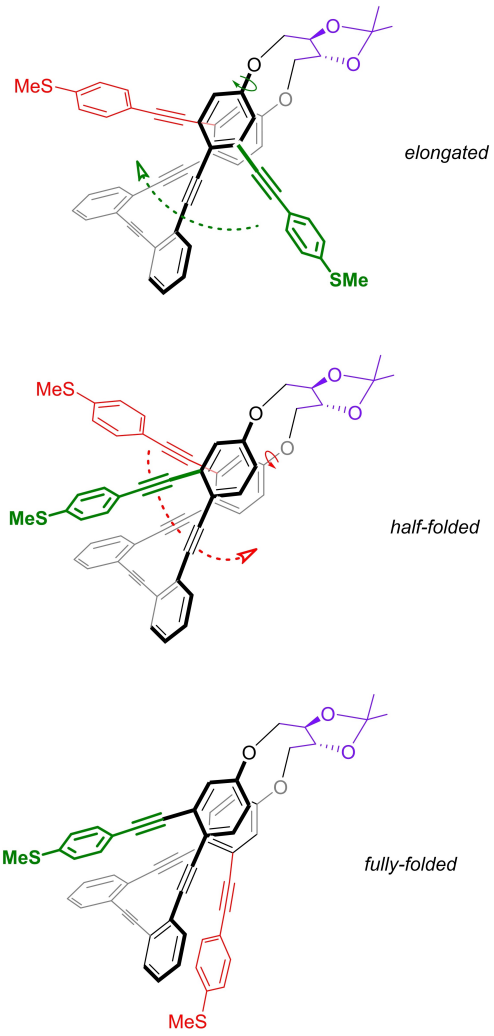

Figure 3. (a) Geometries of the fully-folded, half-folded and elongated geometries of compound (*S*,*S*,*P*)-**2**. The arrows represent the rotation that gives rise to the conformation shown below. Relative populations are 87.8 %, 12.1 % and negilible respectively (see Table S4 for complete conformer analysis).

to determine if (*S*,*S*,*P*)-**2** acts as a potentiometer with well-defined conductance states. This would allow for the possibility of switching between conductance states and, at the same time, modulate the spin polarization. Full details of sample preparation and methodology are given in Section 6 of the Supporting Information. The 2D conductance histograms, obtained from the conductance versus distance (*G*-*z*) traces recorded during the retraction of the tip from contact with the surface, for both compounds are summarized in Figure 4. The figure shows the results after an automated program is used to identify those traces displaying conductance plateaus (see Supporting Information, section 6).

For model structure **1**, we found that 12 % of the recorded traces contain a clear molecular conductance signal that gives rise to two conductance clouds in the 2D histogram representation (Figure 4a). A further subdivision of the traces was performed using an unsupervised k-means clustering process[28] (Figure 4b) which shows that the two

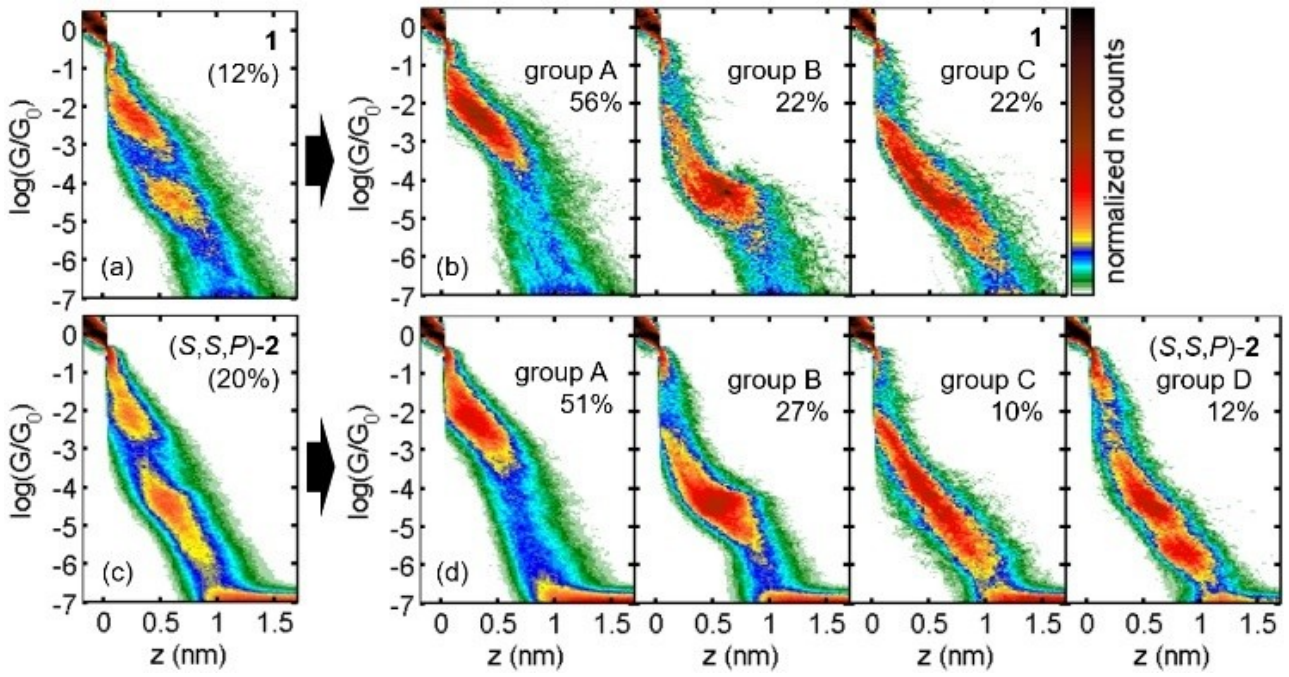

Figure 4. 2D histograms for traces displaying plateaus of compounds **1** and (*S*,*S*,*P*)-**2**. Left panel: histograms obtained from all traces displaying plateaus identified by an automated program. The percentage of these traces with respect to the total number of recorded ones is indicated in brackets. Right panel: subdivision of these traces in several groups using a clustering analysis.

clouds arise from independent set of traces. Generally, there is only one plateau per trace (examples of individual plateaus are shown in the Supporting Information, Figure S17). It is not impossible to find individual *G*-*z* traces that contain plateaus in both states, but the statistical significance of this is very low. The fact that we observe two independent clouds suggests that **1** can initially be trapped in two different stable folded conformations with practically no transition from one to the other during stretching. For *G*-*z* traces with high G signals (group A), we find that the conductance clouds have a significant slope ($\approx$0.37 Å^{-1}), which is very different from the typical horizontal clouds of compounds that cannot fold, like linear OPEs,[6] suggesting that the plateaus derive from a folded conformation of **1** which gets stretched and elongated during the separation of the electrodes in a similar way to previously suggested.[8] Transport seems to proceed with a strong through-space contribution such that, as the molecule elongates, modifying the intramolecular through-space π-overlap or even the overlap with the gold electrodes, reduces the overall conductance. On the other hand, the second cloud at lower G is formed by traces with two different profiles, those with conventional flat plateaus (group B) and those with again a pronounced slope (group C). These observations suggest that the folded conformation responsible of the low-G cloud can be less susceptible to stretching than that of high-G one. Figure 5a–c shows the corresponding 1D histograms and plateau-length distributions from the 3 subgroups of traces separately.

We next turn to the covalently-stapled compound (*S*,*S*,*P*)-**2** that combines both, fixed helicity and chiral

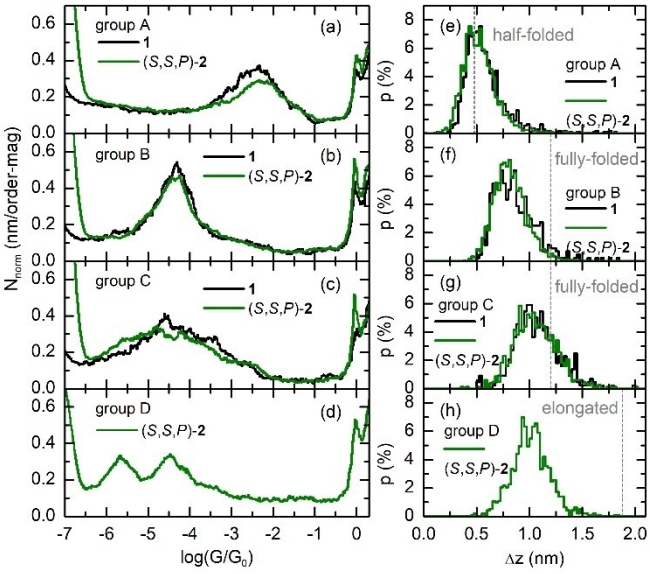

Figure 5. Comparison of 1D histograms (a–d) and plateau-length distributions (e–h) for the same groups of traces of compounds **1** and (*S*,*S*,*P*)-**2** shown in Figure 4.The theoretical expected plateau length for the half-folded, fully-folded and elongated geometries have been added to the Figures as vertical grey dashed lines for comparison.

information. (*S*,*S*,*P*)-**2** is pre-folded in one conformation (as previously described) so that it cannot completely unfold during stretching. In Figure 4c, we observe two main conductance clouds, which are very similar to those of **1**, however the probability of molecular junction formation is almost double, which supports the idea of the staple

stabilizing the folded conformations. Contrary to **1**, (*S*,*S*,*P*)-**2** shows an additional signal at conductance values below 10^{-5} G_0. In fact, the clustering subdivision of the traces shows that for (*S*,*S*,*P*)-**2**, 12 % of the traces with plateaus show flat plateaus between 10^{-6} G_0 and 10^{-5} G_0 (group D). Plateaus at these values were hardly detectable for **1**, indicating that this particular conformation requires a staple in order to appear experimentally. It is noteworthy that these lower conductance plateaus frequently appear after a plateau between 10^{-5} G_0 and 10^{-4} G_0, suggesting a transition between two stable conformations during the stretching.

The similarities of the conductance and length distributions of compounds **1** and (*S*,*S*,*P*)-**2** suggest that very similar conformations are being formed, albeit via different mechanisms given that **1** is unstapled. A possible reason for this is the well-known propensity for *o*-OPEs to act as ligands for carbophilic metals like silver.[22,23] Incorporation of such metals into the molecular structure causes them to adopt defined, stable, 3D structures. We anticipate that gold, with its known capability to coordinate to alkynes in catalytic applications,[29] could behave in a similar fashion. Adatoms originating from the gold electrodes could incorporate themselves into the structure of **1**, causing it to adopt stable, folded structures similar to (*S*,*S*,*P*)-**2** (fully-folded or half-folded).The latter can also incorporate gold in its structure but resulting in no changes in this case as the helix is already fixed by the staple. We have previously observed such behavior for Ag-*o*-OPE complexes.[23] This would also account for the presence of well-defined BJ signal for our unstapled compound in contrast to previously investigated but without alkyne groups.[8] Despite the similarities in conductance between **1** and (*S*,*S*,*P*)-**2**, it is important to state that enantiopure folded conformations can only occur in the stapled compound.

To shed light about the origin of the different conductance groups observed for (*S*,*S*,*P*)-**2**, we performed electron-transport calculations based on density functional theory (DFT) and non-equilibrium Green's functions. For this, we used the code ANT[30] which interfaces with Gaussian 09[31] and also includes an implementation of the spin-orbit coupling (SOC) based on optimized gaussian basis sets.[32] All calculations were based on the GGA + U method (see the Supporting Information for details on both implementations).

Taking into account the conformation flexibility of (*S*,*S*,*P*)-**2**, we built three different model geometries corresponding to the elongated, half-folded and fully-folded geometry (Figure 6a–c).

It is worth noting that the three geometries considered should be regarded as key selected cases. This set does not include all the possible conformations induced by thermal fluctuations and by the stretching process. Thus, we only considered end-to-end configurations in which the molecule is linked to the electrodes via the terminal S. Only the top-binding geometry (in which the S atom is linked to only one Au atom) was studied, as it is known to be preferred by the SMe group when binding to gold.[33]

The transmission as a function of energy is shown in the three model configurations in the upper panel of Figure 6d

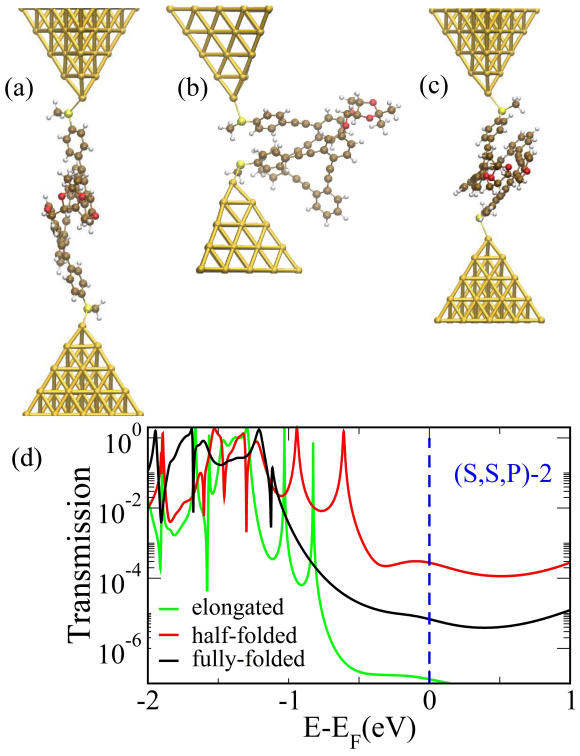

Figure 6. (a)–(c) Binding geometries considered of (*S*,*S*,*P*)-**2**. (d) Transmission (upper panel) and polarization (lower panels) as a function of energy for (*S*,*S*,*P*)-**2**, for the geometries denoted as elongated (a), "half-folded" (b) and "fully-folded" (c).

(see Figure S16 for the corresponding curves for compound 1). The fact that the occupied states are much closer to the Fermi level than the unoccupied states indicates that the electrons flow through the tail of the HOMO for all configurations (the density of states is reported in the Supporting Information). More importantly, the three conformations are found to give rise to three well separated conductance values. The highest electrical conductance, given by the transmission at the Fermi level, is found for the half-folded geometries (2.7×10^{-4} G_0). This is not surprising, given the shortest Au–Au distance in this geometry (0.89 nm) as compared to the others. It is worth noting that, despite most of the molecule being displaced with respect to Au–Au axis, its contribution is still significative as the HOMO is partially localized on the S atoms. The fully-folded structure (1.63 nm) exhibits a conductance value of 6.8×10^{-6} G_0, while the lowest value (1.3×10^{-7} G_0) is found for the elongated structure and can be ascribed to the largest Au–Au distance (2.33 nm).

Table 1 shows the comparison with the experimentally determined conductance values, presenting reasonable matching taking into account the uncertainties about the real geometry at the junction. We assigned the highest conductance group with the half-folded conformation (structure represented in Figure 3 and Figure 6b). The middle group can be associated with the fully-folded conformation (Figure 6c) whilst the lowest observable group can be (tentatively) assigned to the elongated structure (Figure 6a)

Table 1: Experimental mean conductance values for three conductance peaks of (*S*,*S*,*P*)-**2**, compared with the theoretical predicted conductance for molecular junctions of the most probable folded conformations (see previous section).

Experiments		Theory	
Group A	1.6×10^{-3} G_0	2.7×10^{-4} G_0	half-folded
Group B	2.1×10^{-5} G_0	6.8×10^{-6} G_0	fully-folded
Group D	1.3×10^{-6} G_0	1.3×10^{-7} G_0	elongated

which evolves from the fully-folded structure. These assignments can account for all experimental observations. It explains why we do not experimentally observe interconversion between the high and medium conductance groups, which correspond to the (shorter) half-folded and (longer) fully-folded geometries. Such a transition is not observed in the relaxed scan performed while increasing S–S distance starting either from the half-folded or the fully-folded structure (see Figure S13). A roughly 180° rotation of one of the phenyl rings attached to the staple is not possible due to steric hindrance and the two scans suggest that it is possible to change the reciprocal orientation of the three diphenylacetylene groups by rotating the one opposite to the staple. This however requests a high amount of energy and a S–S distance significantly longer than the one of the fully-folded state. The continuous separation of the electrodes means it is unlikely that the S–S distance increases and then decreases during stretching when the S-atoms are anchored to the electrodes, so the fully-folded structure cannot reach an half-folded geometry during such process, but also starting from the half-folded situation the system does not get fully folded. On the other hand, the fully-folded conformation, with the two S atoms initially at higher distance, can conceivably convert to the elongated geometry via a progressively increasing S–S distance, which provides an explanation of the signal in Group D (Figure 4).[34] This transition occurs quite often for (*S*,*S*,*P*)-**2** (in 12 % of the molecular junctions) while it seems hardly to happen for **1**, which may reflect the difference in the way the two compounds are folded (covalently-stapled in (*S*,*S*,*P*)-**2** versus Au-adatom stabilized in **1**). In addition to the conductance values, the comparison between the experimental and theoretical plateau length distribution (Figure 5e–h) also support the conformation assigned to each conductance cloud (See Section 6 in Supporting Information for complete analysis of the traces).

The enantiopurity of compound (*S*,*S*,*P*)-**2** makes it a potential candidate to study the CISS effect. It is worth noting that no studies have been carried out with simple organic molecules at unimolecular level and uncertainties about such potential exist. It is also worth noting that predicting CISS in real systems, taking into account the global complexity of both molecule and electrodes, is challenging and almost unknown in the literature (a few previous studies considered idealized helical structures).[15–18] Within this context, in this final part of the manuscript we have evaluated such feasibility analyzing the spin polarization arising in each model conformations. We would like to stress that the use of optimized basis sets was found to be very important for an accurate study of this effect. In particular, a correct description of the electronic structure of the leads is crucial for reproducing SOC-induced splitting in the band structure. Use of non-optimized basis sets can lead to incorrect values of the polarization. In Figure 7, the polarization as a function of energy for compound (*S*,*S*,*P*)-**2** in the three configurations is shown. For each configuration, we show the polarization in the three cartesian directions for the spin injections, z being the electron-transport direction. We observe that the direction with the highest polarization changes depending on the geometry. The fact that spin polarization can be significant in perpendicular directions to the transport direction in molecules is an important result that has been almost ignored in the literature. This could be especially important in establishing the conditions for the co-existence and simultaneous measurements of spin polarization (mostly associated to the z-component) and spin coherence (mostly related to the x- and y-components), a non-trivial problem because the three components of the polarization vector inherit their non-commutative character from the Pauli spin matrices.[35]

The polarization curves of this compound (Figure 7), reveal that the position of the peaks generally coincides with that of the transmission resonances. However, the amplitude of the polarization peaks seems to depend on the energy range they fall in: while the polarization is generally low for energies closer to the Fermi level (which correspond to the energy window of the Au *s* states), it is much higher, reaching a quite remarkable value of up to 0.4, in the energy range corresponding to the Au *d* states. Similar polarizations were also observed for compound **1** (Figure S16). Indeed, the overall polarization is dictated by an interplay between the intrinsic symmetrical properties of the molecular orbitals

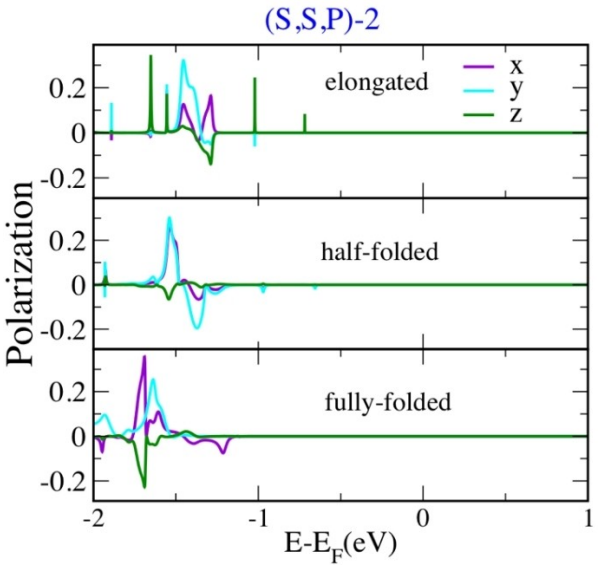

Figure 7. Polarization for the (*S*,*S*,*P*)-**2** junctions in the three cartesian directions is displayed, z being the electron-transport direction and xy being the plane perpendicular to it.

and the symmetry of the orbitals in the electrode they are aligned with. An additional demonstration that part of the spin-orbit interaction involved in the CISS effect is inherited from the gold electrode.[36]

For a more detailed discussion about the role of the gold electrodes, see ref.18. Finally, one should bear in mind that the conformational changes induced in the molecule by the elongation of the junction might affect the polarization values significantly. Note that the non-optimal polarization observed in the energy range closer to the Fermi level (with values between 10^{-8} and 0.03) means that low-bias measurements would hardly be able to detect it and larger voltage would be needed in order to observe polarization for this system.[37] Although globally this chiral potentiometer is able to act as spin filtering material in which the polarization can be modified synchronically with conductance, no significant polarization is expected in the voltage windows used in typical STM-BJ experiences.

Conclusion

We have evaluated the behavior of two *o*-OPEs as potentiometers, observing that both **1** and (*S*,*S*,*P*)-**2** form stable molecular junctions via formation of (Me)S–Au bonds to the electrodes. Despite the behavior of both is very similar, suggesting that both adopt similar conformations in the junction, we endorse a double role of the chiral staple present in (*S*;*S*,*P*)-**2**.

Firstly, (*S*,*S*,*P*)-**2** yields more defined conductance plateaus and a high percentage of them, coinciding with the most energetically favorable conformations and with a conductance variation up to three orders of magnitude. In addition, the staple restricts the conformation space, and we find that the two dominant geometries are a fully-folded and a half-folded arrangement, related via rotation of one of the MeS–Ph–C≡C–Ph-arms. The two structures do not appear to interconvert in the junction, which can be understood due to the binding of the two SMe groups to the electrodes. On the other hand, we observe a transition between two states consistent with pulling the fully folded geometry into an elongated conformation. This behavior leads to several distinct conductance groups with the potential of switching between them. Thus, we have achieved our goal of developing a chiral compound that can also act as a multi-state potentiometer.

Secondly, the persistence of the absolute configuration of the helix during the entire process introduces chirality in the design of potentiometers, thus allowing the creation of potential CISS-based control of intensities of different electronic spins. The polarization computed for compound (*S*,*S*,*P*)-**2** makes it an interesting starting point for the future employment of chiral molecules as active elements in spin-filtering devices. All these results were supported by state-of-the-art theoretical calculations. Further development will be needed in the future to be able to detect the CISS effect in these kinds of single-molecule junctions.

Acknowledgements

We thank the Spanish MICIN for the "María de Maeztu" Programme for Units of Excellence in R&D (grant No. CEX2018-000805-M). Financial support from MCIN/AEI/10.13039/501100011033 is acknowledged by L.A.Z. (grant PID2021-125604NB-I00), E. L. (PID2021-127964NB-C21), D. M. and J. M. C. (PID2020-113059GB-C21), A. M. (PID2021-127964NB-C22) and A. O. G. for her FPU contract (FPU16/02597). We also thank the Universidad Autónoma de Madrid and the Comunidad de Madrid (grants No. SI3/PJI/2021-00191, S2018/NMT-4321 through the Nanomag COST-CM Program and E.L. for Atracción de Talento grant 2019-T1/IND-16384). J. J. P. acknowledges financial support from Spanish MICINN (PID2019-109539GB-C43) and the Generalitat Valenciana through Programa Prometeo/2021/01. This research was also funded by FEDER/Junta de Andalucía-Consejería de Economía y Conocimiento/P20 00162 and the Visiting Scholar Program in the University of Granada. IMDEA Nanociencia acknowleges support from the 'Severo Ochoa' Programme for Center of Excelence in R&D (CEX2020-001039-S). G.L. acknowledges financial support from Italian MIUR through the PRIN program, grant 2017 A4XRCA. VM acknowledges the support of the W.M Keck Foundation through the grant "Chirality, spin coherence and entanglement in quantum biology. The authors thankfully acknowledge the computer resources, technical expertise and assistance provided by the Centro de Computación of Universidad Autónoma de Madrid and the high performance computing (HPC) facility at Unisa. Funding for open access charge: Universidad de Granada / CBUA.

Conflict of Interest

The authors declare no conflict of interest.

Data Availability Statement

The data that support the findings of this study are available in the supplementary material of this article.

Keywords: Chiroptical Properties · Helical Potentiometer · Scanning Tunneling Microscope · Spin Filtering · Transport Calculations

[1] a) T. A. Su, M. Neupane, M. L. Steigerwald, L. Venkataraman, C. Nuckolls, *Nat. Rev. Mater.* **2016**, *1*, 16002; b) J. L. Zhang, J. Q. Zhong, J. D. Lin, W. P. Hu, K. Wu, G. Q. Xu, A. T. S. Weeb, W. Chen, *Chem. Soc. Rev.* **2015**, *44*, 2998–3022.
[2] A. Vezzoli, *Nanoscale* **2022**, *14*, 2874–2884.
[3] J. S. Meisner, M. Kamenetska, M. Krikorian, M. L. Steigerwald, L. Venkataraman, C. Nuckolls, *Nano Lett.* **2011**, *11*, 1575–1579.
[4] T. A. Su, J. R. Widawsky, H. Li, R. S. Klausen, J. L. Leighton, M. L. Steigerwald, L. Venkataraman, C. Nuckolls, *J. Am. Chem. Soc.* **2013**, *135*, 18331–18334.

[5] a) M. Kiguchi, T. Ohto, S. Fujii, K. Sugiyasu, S. Nakajima, M. Takeuchi, H. Nakamura, *J. Am. Chem. Soc.* **2014**, *136*, 7327–7332; b) M. Iwane, S. Fujii, T. Nishino, M. Kiguchi, *J. Phys. Chem. C* **2016**, *120*, 8936–8940; c) L.-Q. Pei, J. R. Horsley, J.-W. Seng, X. Liu, Y. Q. Yeoh, M.-X. Yu, X.-H. Wu, A. D. Abell, J.-F. Zheng, X.-S. Zhou, J. Yu, S. Jin, *ACS Appl. Mater. Interfaces* **2021**, *13*, 57646–57653; d) Z. Zhu, H. Qu, Y. Chen, C. Zhang, R. Li, Y. Zhao, Y. Zhou, Z. Chen, J. Liu, Z. Xiao, W. Hong, *J. Mater. Chem. C* **2021**, *9*, 16192–16198; e) Z. Cai, N. Zhang, M. A. Awais, A. S. Filatov, L. Yu, *Angew. Chem. Int. Ed.* **2018**, *57*, 6442–6448; *Angew. Chem.* **2018**, *130*, 6552–6558; f) M. El Abbassi, P. Zwick, A. Rates, D. Stefani, A. Prescimone, M. Mayor, H. S. J. van der Zant, D. Dulic, *Chem. Sci.* **2019**, *10*, 8299–8305; g) C. Seth, V. Kaliginedi, S. Suravarapu, D. Reber, W. Hong, T. Wandlowski, F. Lafolet, P. Broekmann, G. Royal, R. Venkatramani, *Chem. Sci.* **2017**, *8*, 1576–1591.

[6] a) D. Miguel, L. Álvarez de Cienfuegos, A. Martín-Lasanta, S. P. Morcillo, L. A. Zotti, E. Leary, M. Bürkle, Y. Asai, R. Jurado, D. J. Cárdenas, G. Rubio-Bollinger, N. Agraït, J. M. Cuerva, M. T. González, *J. Am. Chem. Soc.* **2015**, *137*, 13818–13826; b) L. Palomino-Ruiz, P. Reiné, I. R. Márquez, L. Álvarez de Cienfuegos, N. Agraït, J. M. Cuerva, A. G. Campaña, E. Leary, D. Miguel, A. Millán, L. A. Zotti, M. T. González, *J. Mater. Chem. C* **2021**, *9*, 16282–16289.

[7] M. Koike, S. Fujii, H. Cho, Y. Shoji, T. Nishino, T. Fukushima, M. Kiguchi, *Jpn. J. Appl. Phys.* **2018**, *57*, 03EG05.

[8] J. Li, P. Shen, S. Zhen, C. Tang, Y. Ye, D. Zhou, W. Hong, Z. Zhao, B. Z. Tang, *Nat. Commun.* **2021**, *12*, 167.

[9] F. Evers, A. Aharony, N. Bar-Gill, O. Entin-Wohlman, P. Hedegård, O. Hod, P. Jelinek, G. Kamieniarz, M. Lemeshko, K. Michaeli, V. Mujica, R. Naaman, Y. Paltiel, S. Refaely-Abramson, O. Tal, J. Thijssen, M. Thoss, J. M. van Ruitenbeek, L. Venkataraman, D. H. Waldeck, B. i. Yan, L. Kronik, *Adv. Mater.* **2022**, *34*, 2106629.

[10] Z. Shang, T. Liu, Q. Yang, S. Cui, K. Xu, Y. Zhang, J. Deng, T. Zhai, X. Wang, *Small* **2022**, *18*, 2203015.

[11] C. D. Aiello, J. M. Abendroth, M. Abbas, A. Afanasev, S. Agarwal, A. S. Banerjee, D. N. Beratan, J. N. Belling, B. Berche, A. Botana, J. R. Caram, G. L. Celardo, G. Cuniberti, A. Garcia-Etxarri, A. Dianat, I. Diez-Perez, Y. Guo, R. Gutierrez, C. Herrmann, J. Hihath, S. Kale, P. Kurian, Y.-C. Lai, T. Liu, A. Lopez, E. Medina, V. Mujica, R. Naaman, M. Noormandipour, J. L. Palma, Y. Paltiel, W. Petuskey, J. C. Ribeiro-Silva, J. J. Saenz, E. J. G. Santos, M. Solyanik-Gorgone, V. J. Sorger, D. M. Stemer, J. M. Ugalde, A. Valdes-Curiel, S. Varela, D. H. Waldeck, M. R. Wasielewski, P. S. Weiss, H. Zacharias, Q.-H. Wang, *ACS Nano* **2022**, *16*, 4989–5035.

[12] A. C. Aragonès, A. Martín-Rodríguez, D. Aravena, G. Di Palma, W. Qian, J. Puigmartí-Luis, N. Aliaga-Alcalde, A. González-Campo, I. Díez-Pérez, E. Ruiz, *Angew. Chem. Int. Ed.* **2021**, *60*, 25958–25965; *Angew. Chem.* **2021**, *133*, 26162–26169.

[13] A. C. Aragones, D. Aravena, F. J. Valverde-Muñoz, J. A. Real, F. Sanz, I. Díez-Perez, E. Ruiz, *J. Am. Chem. Soc.* **2017**, *139*, 5768–5778.

[14] A. C. Aragonès, E. Medina, M. Ferrer-Huerta, N. Gimeno, M. Teixidó, J. L. Palma, N. Tao, J. M. Ugalde, E. Giralt, I. Díez-Pérez, V. Mujica, *Small* **2017**, *13*, 1602519.

[15] S. Dalum, P. Hedegård, *Nano Lett.* **2019**, *19*, 5253–5259.

[16] M. S. Zöllner, S. Varela, E. Medina, V. Mujica, C. Herrmann, *J. Chem. Theory Comput.* **2020**, *16*, 7357–7371.

[17] Y. Liu, J. Xiao, J. Koo, *Nat. Mater.* **2021**, *20*, 638–644.

[18] W. Dednam, M. A. García-Blázquez, L. A. Zotti, E. B. Lombardi, C. Sabater, S. Pakdel, J. J. Palacios, arXiv:2211.04830.

[19] J. Nejedlý, M. Šámal, J. Rybáček, I. G. Sánchez, V. Houska, T. Warzecha, J. Vacek, L. Sieger, M. Buděšínský, L. Bednárová, P. Fiedler, I. Císařová, I. Starý, I. G. Stara, *J. Org. Chem.* **2020**, *85*, 248–276.

[20] a) M. Kettner, B. Göhler, H. Zacharias, D. Mishra, V. Kiran, R. Naaman, C. Fontanesi, D. H. Waldeck, S. Sek, J. Pawlowski, J. Juhaniewicz, *J. Phys. Chem. C* **2015**, *119*, 14542–14547; b) V. Kiran, S. R. Cohen, R. Naaman, *J. Chem. Phys.* **2017**, *146*, 092302; c) C. Hsu, W. M. Schosser, P. Zwick, D. Dulić, M. Mayor, F. Pauly, H. S. J. van der Zant, *Chem. Sci.* **2022**, *13*, 8017–8024; d) S. Mishra, A. K. Mondal, S. Pal, T. K. Das, E. Z. B. Smolinsky, G. Siligardi, R. Naaman, *J. Phys. Chem. C* **2020**, *124*, 10776–10782; e) P. Möllers, S. Ulku, D. Jayarathna, F. Tassinari, D. Nürenberg, R. Naaman, C. Achim, H. Zacharias, *Chirality* **2021**, *33*, 93–102.

[21] L. A. Zotti, J. C. Cuevas, *ACS Omega* **2018**, *3*, 3778–3785.

[22] a) P. Reiné, J. Justicia, S. P. Morcillo, S. Abbate, B. Vaz, M. Ribagorda, A. Orte, L. Álvarez de Cienfuegos, G. Longhi, A. G. Campaña, D. Miguel, J. M. Cuerva, *J. Org. Chem.* **2018**, *83*, 4455–4463; b) A. M. Ortuño, P. Reiné, S. Resa, L. Álvarez de Cienfuegos, V. Blanco, J. M. Paredes, A. J. Mota, G. Mazzeo, S. Abbate, J. M. Ugalde, V. Mujica, G. Longhi, D. Miguel, J. M. Cuerva, *Org. Chem. Front.* **2021**, *8*, 5071–5086.

[23] a) A. Martín-Lasanta, L. Álvarez de Cienfuegos, A. Johnson, D. Miguel, A. J. Mota, A. Orte, M. J. Ruedas-Rama, M. Ribagorda, D. J. Cárdenas, M. C. Carreño, A. M. Echavarren, J. M. Cuerva, *Chem. Sci.* **2014**, *5*, 4582–4591; b) S. P. Morcillo, D. Miguel, L. Álvarez de Cienfuegos, J. Justicia, S. Abbate, E. Castiglioni, C. Bour, M. Ribagorda, D. J. Cárdenas, J. M. Paredes, L. Crovetto, D. Choquesillo-Lazarte, A. J. Mota, M. C. Carreño, G. Longhi, J. M. Cuerva, *Chem. Sci.* **2016**, *7*, 5663–5670.

[24] B. P. Bloom, B. M. Graff, S. Ghosh, D. N. Beratan, D. H. Waldeck, *J. Am. Chem. Soc.* **2017**, *139*, 9038–9043.

[25] S. J. Grimme, *J. Chem. Theory Comput.* **2019**, *15*, 2847–2862.

[26] Gaussian 16, Revision C.01, M. J. Frisch, et al., Gaussian, Inc., Wallingford CT, **2016**.

[27] S. Grimme, J. Antony, S. Ehrlich, H. Krieg, *J. Chem. Phys.* **2010**, *132*, 154104.

[28] L. Palomino-Ruiz, S. Rodríguez-González, J. G. Fallaque, I. R. Márquez, N. Agraït, C. Díaz, E. Leary, J. M. Cuerva, A. G. Campaña, F. Martín, A. Millán, M. T. González, *Angew. Chem. Int. Ed.* **2021**, *60*, 6609–6616; *Angew. Chem.* **2021**, *133*, 6683–6690.

[29] For a review about gold coordination to alkynes see: R. Dorel, A. M. Echavarren, *Chem. Rev.* **2015**, *115*, 9028–9072.

[30] a) D. Jacob, J. J. Palacios, *J. Chem. Phys.* **2011**, *134*, 044118; b) J. J. Palacios, D. Jacob, A. J. Perez-Jimenez, E. S. Fabian, E. Louis, J. A. Verges. https://www.simuneatomistics.com/; c) J. J. Palacios, A. J. Pérez-Jiménez, E. Louis, E. SanFabián, J. A. Vergés, *Phys. Rev. B* **2002**, *66*, 035322.

[31] M. J. Frisch, et al., Computer code GAUSSIAN09, Revision C.01, Gaussian, Inc. Wallingford, CT, **2009**.

[32] W. Dednam, L. A. Zotti, S. Pakdel, E. Lombardi, J. Palacios, *Proc. 65th Annual Conf. South African Institute of Physics* **2022**, *65*, 25–30.

[33] a) T. A. Su, H. Li, M. L. Steigerwald, L. Venkataraman, C. Nuckolls, *Nat. Chem.* **2015**, *7*, 215–220; b) M. Kamenetska, M. Koentopp, A. C. Whalley, Y. S. Park, M. L. Steigerwald, C. Nuckolls, M. S. Hybertsen, L. Venkataraman, *Phys. Rev. Lett.* **2009**, *102*, 126803.

[34] The contribution to the geometry space of the elongated geometry is predicted to be low in solution, however, in a single molecule junction the force acting on the molecule due to binding to the electrodes may be enough to stretch the molecule into this conformation.

[35] a) M. W. Rahman, M. C. Mañas-Torres, S. Firouzeh, J. M. Cuerva, L. Álvarez de Cienfuegos, S. Pramanik, *ACS Nano* **2021**, *15*, 20056–20066; b) W. Rahman, M. C. Mañas-Torres, S.

Firouzeh, S. Illescas-Lopez, J. M. Cuerva, M. T. Lopez-Lopez, L. Álvarez de Cienfuegos, S. Pramanik, *ACS Nano* **2022**, *16*, 16941–16953.
[36] V. V. Maslyuk, R. Gutierrez, A. Dianat, V. Mujica, G. Cuniberti *J. Phys. Chem. Lett.* **2018**, *9*, 18, 5453–5459.
[37] We would like to stress that, although our calculations allow us to evaluate the spin-polarization of the current in non-magnetic two-terminal devices, here we have not addressed how to verify the predicted spin-polarization in a laboratory. This would certainly require the employment of more elements in the circuit such as magnetic electrodes, additional terminals, nodes where spin accumulation can be measured, finite bias, or dephasing. This is beyond the current scope of this work, which aims at exploring the suitability of these compounds for CISS-based experiments.

Manuscript received: December 16, 2022
Accepted manuscript online: February 20, 2023
Version of record online: March 6, 2023